Diameter of basalt columns derived from fracture mechanics bifurcation analysis

H.-A. Bahr,[1,*] M. Hofmann,[1] H.-J. Weiss,[2] U. Bahr,[3] G. Fischer,[4] and H. Balke[1]
[1]*Institut für Festkörpermechanik, Technische Universität Dresden, Mommsenstr. 13, D-01062 Dresden, Germany*
[2]*Fraunhofer-Institut für Werkstoff- und Strahltechnik, Winterbergstr. 28, D-01277 Dresden, Germany*
[3]*Institut für Theoretische Physik, Technische Universität Dresden, Mommsenstr. 13, D-01062 Dresden, Germany*
[4]*Lehrstuhl für Qualitätswesen, Universität Dortmund, Joseph-von-Fraunhofer-Str. 20, D-44227 Dortmund, Germany*
(Received 23 January 2009; published 5 May 2009)

The diameter of columnar joints forming in cooling basalt and drying starch increases with decreasing growth rate. This observation can be reproduced with a linear-elastic three-dimensional fracture mechanics bifurcation analysis, which has been done for a periodic array of hexagonal columnar joints by considering a bifurcation mode compatible with observations on drying starch. In order to be applicable to basalt columns, the analysis has been carried out with simplified stationary temperature fields. The critical diameter differs from the one derived with a two-dimensional model by a mere factor of 1/2. By taking into account the latent heat released at the solidification front, the results agree fairly well with observed column diameters.

DOI: 10.1103/PhysRevE.79.056103 PACS number(s): 46.50.+a, 47.54.−r, 91.55.−y

I. INTRODUCTION

The well-known conspicuous basalt columns with preferably hexagonal cross sections give rise to wonder and an urge for explanation. The preference for hexagons has been quantified in [1,2]. Basalt columns originate from crack propagation caused by thermal contraction of solidified lava.

A similar columnar type of disintegration is observed in other contracting solids, such as sandstone [3–5] and drying starch slurry, for example. The latter has repeatedly been used as a model substance for investigating the phenomenon [6–13]. The shrinkage cracks starting from the surface in a random distribution turn into a more regular polygonal configuration, with hexagons prevailing, while propagating into the depth, as has been observed in [13] with computer tomography; see the schematic drawing in Fig. 1. This technique has also revealed that the column diameter may abruptly increase locally by way of two or three columns merging into one. This is brought about by a rearrangement of the crack configuration in the course of propagation, as shown later in Fig. 4(a), for example, where a knot of the network, together with the three sections of the crack front it is made of, is seen to stop, which finally leads to a coarser mesh, or larger columns. Such coarsening of developing crack patterns is also observed in basalt before stationary crack propagation forms columns with constant diameter [14–18].

The maturation process has been simulated with two-dimensional (2D) models (in planes normal to the growth direction) by variation of a Voronoi tessellation [1], by minimizing an energy functional [2,19], or with a three-dimensional (3D) spring network model [20]. The tendency toward hexagon formation is reproduced with the 2D models. The merging of two or three columns into one is also seen in Fig. 3 of [19]. Coarsening phenomena in thermal shock crack patterns are the subject of several theoretical papers [21–26].

The observed coarsening process is connected with a reduction in randomness. This phenomenon has been modeled in [27] and, with a 3D stress analysis by means of finite-element method (FEM), in [28].

Long columns with virtually no variation in cross section *suggest the idea of a steady-state process* for their formation. Such process is expected at depths where cooling from the surface becomes negligible compared to convective heat transfer. The convective flow could be driven through coherent porosity in the basalt [16,29] or through the gaps between the columns [1,18,30]. Steady-state temperature fields were measured in boreholes during solidification of the Kilauea Iki lava lake in Hawaii for 12 years [29]. In the model experiment with drying starch a similar regime was established by controlling the evaporation rate of the liquid [11].

In view of the fact that the phenomenon covers a size range from millimeters to meters at least, the question arises as to *which parameters determine the diameter*. In [1,16] the diameter is assumed to be inversely proportional to the steady-state propagation velocity of the cracks. This is approximately realized with starch columns [11] and was calculated in [31] with a linear-elastic steady-state 2D model [in planes $x=$const in Figs. 2 and 8(a)]. Information from mea-

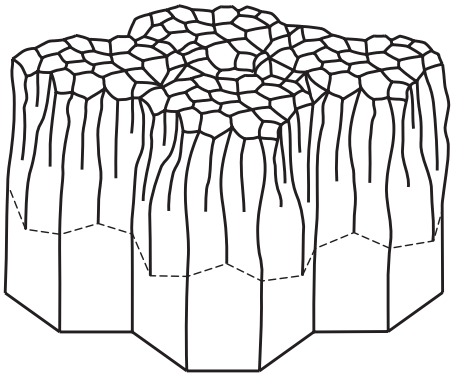

FIG. 1. Schematic illustration of coarsening and reduction in randomness in a crack network during propagation into depth, leading to hexagonal columns.

*Author to whom correspondence should be addressed; hans-achim.bahr@tu-dresden.de

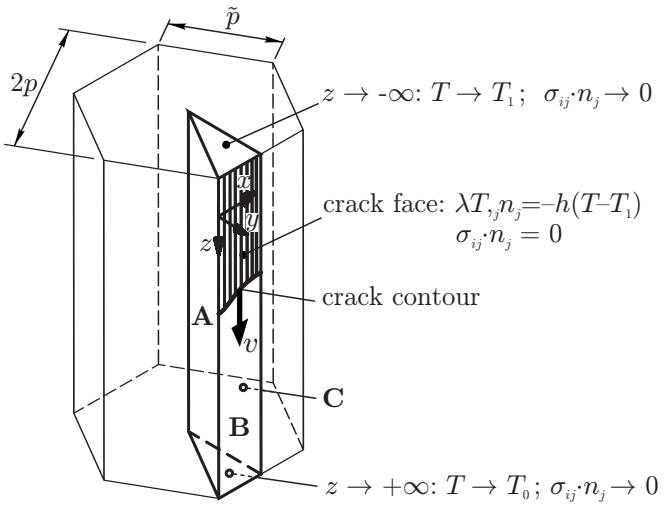

FIG. 2. Element of a periodic array of hexagonal columns with thermomechanical boundary conditions. Only a twelfth part of a column has to be considered which is a three-sided prism with faces A and C and the third side including the shaded crack face up to the crack contour and the ligament face B below it. The crack contour is moving with the velocity v. Symmetry implies $T_{,j} n_j = 0$, $u_j n_j = 0$, and vanishing of the in-plane component of the traction vector, $t_i = \sigma_{ij} n_j$, at faces A, B, and C with the normal vector n_j directed outward.

sured stria heights on the columns has confirmed the above relation, as recently published in [18]; see Sec. V. In connection with a discussion of the approach taken in [31], the idea was favored in [27,28] "that the typical width of the columns is set by the typical distance between cracks at the surface, and it is not modified with the further penetration … since in this (3D) case all fractures form a connected crack structure, and this generates an additional tendency to stabilize the crack front." In contradiction to that idea, our present 3D fracture mechanics bifurcation analysis shows that a minimum column diameter can be derived from calculations based on the steady-state regime.

A linear-elastic thermomechanical 3D model for a periodic array of hexagonal columns, with the crack network making up the columns while propagating in a stationary way, is proposed in Sec. II. The fracture mechanics basic solution of the crack front is given in Sec. III. A particular bifurcation mode ansatz with three columns merging into one is used in Sec. IV to calculate the critical diameter of basalt columns. In Sec. V, the results are compared with observation. It is emphasized that fairly good agreement is obtained only if the heat released during solidification is taken into account. Further conclusions are discussed in Sec. VI.

II. 3D THERMOMECHANICAL MODEL

As schematically shown in Fig. 1 coarsening of an initial crack network precedes the stationary growth of columns. With the cracks advancing, the conductive heat flow to the external surface decreases, and one can assume that convective cooling finally prevails [18]. Crack propagation becomes slower until supposedly a regime of (nearly) steady-state, self-driven column formation with constant velocity is reached. This serves as a justification to do the analysis with constant velocity.

As has been observed with computer tomography [13], the spacing becomes more uniform while the cracks are propagating, which is equivalent to a mutual "repulsion" of neighboring cracks. This is intuitively understandable since the elastic energy available for release during propagation is higher for wider spacing. The tendency toward uniform spacing implies a tendency toward an array of hexagonal columns with equal diameters, which can be approached surprisingly well in reality.

We extend the 2D model used in [31] to a 3D model and assume an idealized periodic array of hexagonal columns (Fig. 2) generated by a crack front moving with the constant velocity v in z direction. There are reasons to restrict the analysis to hexagonal columns: Hexagonal columns are the most abundant ones in the natural column arrays with nonperfect symmetry [1,2]. This justifies the tentative assumption that configurations other than the periodic network of hexagonal meshes are intrinsically unstable in propagation. The validity of this assumption cannot be verified for all configurations, of course. As one example, the periodic network of quadratic meshes has been chosen to prove its instability in propagation, which has been done with 3D stress analysis by means of FEM [28].

In Fig. 2 we assume that the columns extend from $z=-\infty$. The origin of the coordinate system is chosen at some distance from the crack contour. $2p$ is called column diameter, and $\tilde{p}=2p/\sqrt{3}$ is column side width. The inhomogeneous temperature field $T(x,y,z)$ is governed by the heat diffusion with constant thermal diffusivity D, which reads

$$\nabla^2 T + \frac{v}{D} T_{,z} = 0 \tag{1}$$

in the frame of reference moving with the velocity v of the crack contour. $(\,)_{,i}$ means the derivative with respect to x, y, or z.

The stresses σ_{ij} and displacements u_i for linear-elastic isotropic material are described through the equilibrium condition (without gravity) and the constitutive law:

$$\sigma_{ij,i} = 0, \quad \sigma_{ij} = \sigma_{ji},$$

$$\sigma_{ij} = -\frac{E}{1-2\nu}\alpha(T-T_0)\delta_{ij} + \frac{E}{1+\nu}\left[\frac{1}{2}(u_{i,j}+u_{j,i}) + \frac{\nu}{1-2\nu}\delta_{ij}u_{k,k}\right]. \tag{2}$$

Here Einstein's sum rule is applied. The temperature T_0 refers to the reference state where no thermal stress is present. T_0 is realized far ahead of the columns for $z \to \infty$. E, ν, and α are Young's modulus, Poisson's ratio, and the thermal-expansion coefficient of the material. Equations (1) and (2) are solved with the thermomechanical boundary conditions as shown in Fig. 2 by using FEM [32]. Here convective cooling within the cracks is assumed to be the driving force of crack propagation [1,30]. Crack-aided convective cooling

is discussed in more detail in [18] and will be described as in [31] by cooling the crack faces with an effective heat transfer coefficient h,

$$\lambda T_{,j} n_j = -h(T - T_1), \tag{3}$$

in our simplified temperature model. Here λ means the heat conductivity of basalt, and $T_{,j} n_j$ is the derivative in outward normal direction n_j of the crack face. T_1 is maintained in the interior of the cracks and can be regarded as coolant temperature and is realized in the column for $z \to -\infty$ (see Fig. 2).

III. FRACTURE MECHANICS BASIC SOLUTION

Steady-state crack propagation implies that everywhere on the moving crack front the energy released per crack face increment, G, equals the energy consumed per crack face increment, G_c,

$$G = G_c. \tag{4}$$

Where

$$G \leq G_c \tag{5}$$

on the crack front, propagation stops. (As crack propagation is irreversible for reasons lying beyond fracture mechanics, cracks cannot become shorter.) The symmetry of the array of hexagonal columns implies that there is no other than mode I crack opening; hence K_I is the only stress intensity factor contributing to G [33]:

$$G = \frac{1 - \nu^2}{E} K_I^2. \tag{6}$$

K_I has been calculated by the crack opening displacement component $u_I(r)$ perpendicular to the crack face [33]:

$$K_I = \frac{E}{4(1 - \nu^2)} \lim_{r \to 0} \sqrt{\frac{2\pi}{r}} u_I(r). \tag{7}$$

Here r means the distance from the crack contour within the crack face shown schematically in Fig. 2.

The crack contour is found from G=const [not yet fixed to G_c as in Eq. (4)] calculated by means of FEM and iteration with the gradient method described in [34]. The calculated crack contours $\Delta a(x) = a(x) - a(\tilde{p}/2)$ are given in Fig. 3(b). The crack length $a(x)$ is not defined here but the difference is. It is seen that the front is most advanced at the nodes of the hexagonal network because these are cooled via three cracks instead of one.

The energy release rates calculated for this 3D problem,

$$G = \frac{E(\alpha \Delta T)^2 p}{1 - \nu} g\left(\frac{vp}{D}, \frac{hp}{\lambda}\right) \tag{8}$$

with $\Delta T = T_0 - T_1$, depend on two dimensionless parameters (see below). The solution of Eq. (8) is called basic solution and can be seen in Fig. 3(a). The limit $g \to 1$ for $vp/D \to 0$ of homogeneous stress follows analytically from the difference between the remote strain energy densities far behind and far ahead of the crack front. The dependence on ν has been confirmed for $v \neq 0$ by FEM calculations.

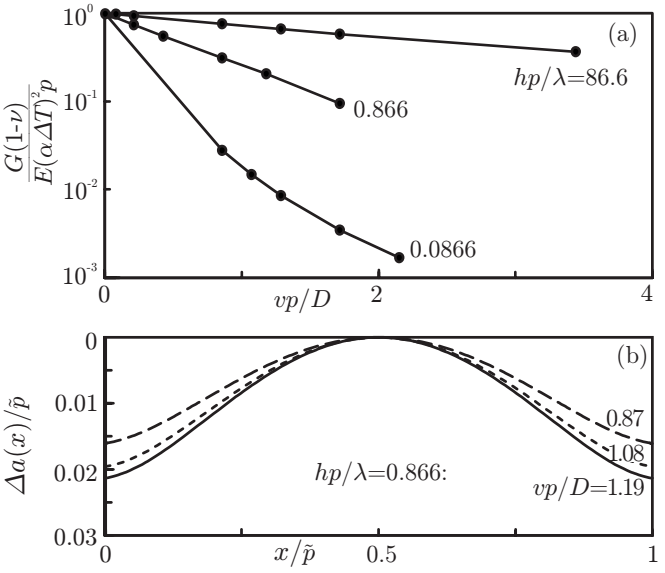

FIG. 3. Basic solution represented by (a) energy release rate G and (b) slightly curved crack contours $\Delta a(x)$ calculated iteratively from G=const.

Our model contains four characteristic lengths, the crack spacing $2p$, the diffusion length D/v in Eq. (1), the cooling length λ/h in cooling boundary equation (3), and from the crack propagation condition $G = G_c$ the length l_0, which is the ratio of crack face energy and stored elastic energy:

$$l_0 = \begin{cases} \dfrac{(1 - \nu) G_c}{E(\alpha \Delta T)^2} & \text{for 3D case} \\ \dfrac{(1 - \nu) G_c}{(1 + \nu) E(\alpha \Delta T)^2} & \text{for 2D case.} \end{cases} \tag{9}$$

Here, l_0 for the 2D case considered in [31] has been included. In our model, l_0 and λ/h are loading parameters from which $2p$ and D/v have to be calculated by means of the two equations $G = G_c$ and the bifurcation criterion discussed below.

IV. 3D BIFURCATION ANALYSIS AND CRITICAL DIAMETER OF BASALT COLUMNS

Experiments with drying starch as shown in Fig. 4(a) (see also movies in [13]) indicate that three columns eventually merge into a larger one. Such merger can be represented by a periodic model as shown in Fig. 4(b). In the following it is shown how to find those critical combinations of the characteristic lengths which make larger columns in this way.

Such phenomenon is equivalent to a mathematical bifurcation, which consists of the coexistence of another solution besides the basic solution. Hence, the problem of determination of the column diameter reduces to finding the bifurcation point (critical combinations of the characteristic lengths) which separates the combinations with only one solution ("basic solution") from those with two solutions ("basic solution" and "bifurcation solution").

In order to find the bifurcation point, one does not need to know the postcritical behavior as such but only its increment

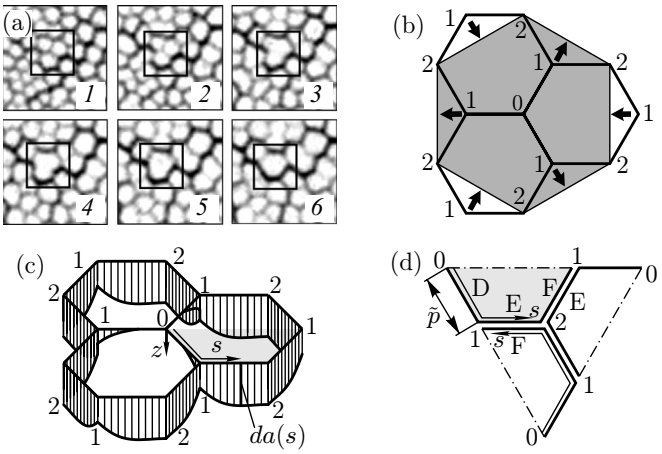

FIG. 4. (a) Sequence of slices through a tomogram of columnar joints growing into the depth of drying corn starch slurry [35]. Note the local phenomenon of three columns merging into one. (b) Idealized interpretation of the local phenomenon in (a): hexagon (shaded) formed by postcritical propagation after a bifurcation-type instability of the hexagonal crack network. (c) Crack contour increment $da(s)$ of the bifurcation mode solution: no propagation in a finite vicinity of point 0 on the crack front. Symmetry and periodicity of the configuration allow the calculations to be restricted to the shaded area, redrawn in (d).

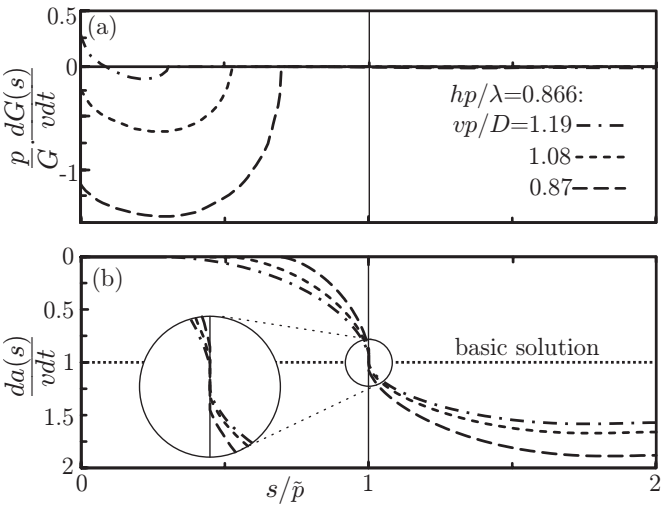

FIG. 5. (a) Energy release rate increment $dG(s)$ and (b) bifurcation mode increment $da(s)$ related to vdt versus position $s/\tilde{p}$ on the crack front for ν=0.21. There is a jump in the crack contour increment at the edge at $s/\tilde{p}$=1 or point 1 in Fig. 4(c). Note that the curves in (b) represent velocities. (For the basic solution the velocity is constant for all s.) The critical value for bifurcation is obtained from the condition $dG(0)$=0 corresponding to Eq. (5) by interpolation as vp/D=1.15.

at the instant of bifurcation. A suitably chosen ansatz for such an increment, $da(s)$ in z direction, depending on position s, is seen in Fig. 4(c). The coordinate s in Fig. 4 runs between four edges (hence it only partially coincides with the coordinate x in Fig. 2). Since $da(s)$ is used to represent the stop of propagation of the crack network at point 0 in Fig. 4(c), it is set to zero there, and tentatively so within an adjacent region. The ansatz for the contour as well as the size of the zero region has to be varied until a solution is found by iteration. According to Eq. (4), the solution is found if the energy release rate increment dG of the crack length increment vanishes everywhere except for the region where $da(s)$ is supposed to be zero and $dG \leq 0$ results from Eq. (5) for stop of crack propagation. Note that the method used to determine the bifurcation point in 3D case, as described in detail in Appendix B, is an extension of the method used to derive a 2D bifurcation in Appendix A.

Calculations were done by means of FEM with a gradient method as described in [34], with the results seen in Fig. 5. As technicality applied for better convergence of the iteration, $da(s)$ has been kept zero where it was tentatively assumed to be so. As seen in Fig. 5(a), this useful restriction in the numerical calculation is not a restriction in reality for the arbitrarily chosen values vp/D=0.87 and 1.08 since dG has turned out to be below zero there, which precludes crack propagation anyway. For another arbitrarily chosen value, vp/D=1.19, the above-mentioned technical restriction is a real one as it pushes dG above zero near point 0 ($s \approx 0$) in contradiction to Eq. (5). So the related curve does not represent a solution but it can be used to find the bifurcation point by quadratic interpolation: vp/D=1.15. Hence, the basic solution is unstable with respect to bifurcation for vp/D <1.15. For the same reason, calculations should converge toward the basic solution for vp/D>1.15.

A few explanatory remarks are adequate here: the incremental extension of the plane crack faces by $da(s)$ is also plane here. This does not pose a restriction, as explained in Appendix D. At point 1, one of the three faces of the crack increment is shorter, as seen in Fig. 5(b). Technical details of the 3D bifurcation analysis can be found in Appendix B. In order to be sure that the bifurcation found here really can lead to the merger of columns, the first incremental step of the subsequent development of the bifurcation solution is considered in Appendix D. There it is shown that the violation of the symmetry of the lattice of hexagons by the presence of the bifurcation solution $da(s)$ gives rise to a $dK_{\mathrm{II}} \neq 0$ with the right sign to curve the crack faces in such a way that the change is toward the formation of a column with a three times larger cross section; see arrows in Fig. 4(b).

The result of the bifurcation analysis can be summarized in this way: for any velocity of steady-state column formation there is a smallest possible column diameter in the sense that for periodic arrays of hexagonal columns any smaller diameter would give rise to a bifurcation-type instability of the process, with three columns merging into a larger one as indicated in Fig. 4. This differs from the expectations in [27] quoted above.

Note that, according to the results in Fig. 5(b), the velocity of the front at the bifurcation point, $da(s)/dt$, which is constant and equal to v for the basic solution, depends on position s for the bifurcation solution. Hence, the transition from the basic solution to the bifurcation solution at vp/D =1.15 involves a jump discontinuity of the velocity.

The critical value vp/D in Fig. 6(a) does not depend on the effective cooling parameter λ/hp, as expected from scaling arguments explained in Appendix C. 3D and 2D results differ only by a factor smaller than 2. From this follows that the effect of the connectivity in the 3D crack network dis-

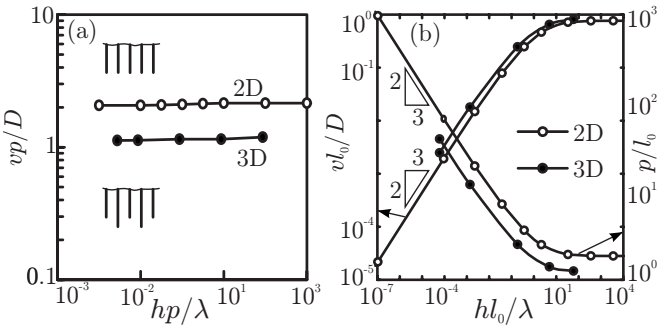

FIG. 6. Stability limits involved in the formation of basalt columns: no bifurcation in the range above the respective curve. (a) critical values for vp/D; (b) bifurcation map representing the complete stability limits of the model for v and p for given loading parameters h/λ and l_0 [see Eq. (9)].

cussed in [27] is not important. (Note that the 2D bifurcation criterion used in [31] has to be replaced by the one derived in Appendix A; hence the results differ slightly from those in [31].)

With the condition $dG(0)=0$ the bifurcation solution is selected from the family of curves in Fig. 5 by interpolation. The propagation condition $G=G_c$ serves as another restriction in parameter space so that both the critical velocities v and half diameters p of the basalt columns are determined [see Fig. 6(b)], with the length l_0 as defined in Eq. (9). The power of 2/3 in Fig. 6(b) has been found in [31] by means of scaling arguments.

We can assume that uniform columns form close to the stability limit in Fig. 6. As discussed in Sec. I in connection with Fig. 1 and in the motivation of the thermomechanical model, coarsening of an initial crack network precedes the stationary growth of columns. In a periodic model of hexagonal columns the coarsening phenomenon could be calculated, in principle, as a nonstationary process involving a sequence of bifurcations, beginning with small column diameters and ending near the critical value in Fig. 6. According to this scenario, the final column diameter should be realized close to the stability limit in Fig. 6, with an uncertainty within a factor of $\sqrt{3}$, and a ratio of 3 for the area in Fig. 4(b).

V. COMPARISON WITH EXPERIMENTS AND IMPROVED MODELS

The dependences shown in Fig. 6 allow the effective heat transfer coefficient h to be eliminated with the result that vp/D is essentially independent of vl_0/D, as shown by the nearly constant curves in Fig. 7. The experimental values in Fig. 7 for $0.1<vp/D<0.27$ are derived from measurements at the solid basalt crust on the Kilauea Iki lava lake on Hawaii (Table I, [11]). There a steady-state temperature field propagating in z direction with $v=6.7\times10^{-8}$ m/s has been measured in boreholes during the course of 12 years. It agrees very well with the model of Hardee [29],

$$T(z)=T_1+\Delta T\frac{1-\exp(-vz/D)}{1-\exp(-vz_0/D)}. \tag{10}$$

This function fulfills Eq. (1) and the boundary conditions $T_1=100$ °C at the specially chosen position $z=0$ (onset of

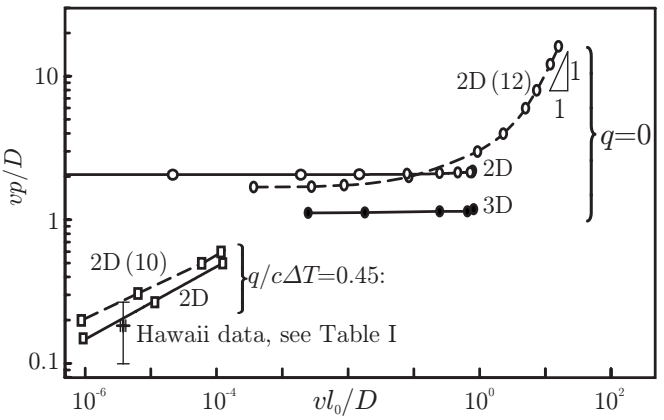

FIG. 7. Stability limits involved in the formation of basalt columns, with and without taking into account the latent heat q released in solidification: no bifurcation in the parameter range above the respective curve. Temperature fields after Eqs. (10) and (12) are used for 2D (10) and 2D (12). The curves labeled 2D and 3D refer to cooling through the cracks. Considering that 3D results could be expected to be lower than the 2D results below left, there is rather good agreement between theory and Hawaii data.

fast convective cooling due to water steam in porous basalt) and $T_0=980$ °C at $z=z_0$ for the solidification temperature of basalt. The distance z_0 follows from the heat flow due to the released latent heat q (Table I) at the solidification front

$$T_{,z}|_{z=z_0}=\frac{qv}{cD},\quad z_0=\frac{D}{v}\ln\left(1+\frac{c\Delta T}{q}\right), \tag{11}$$

with the heat capacity c. In the limit case $q\to0$ the length $z_0\to\infty$ and from Eq. (10) follows

TABLE I. Material parameters of basalt and measured data from Hawaii. (Some parameters slightly deviate from those applied in [18].)

Solidification point T_0	980 °C [16]
Lower temperature T_1	100 °C
$\Delta T=T_0-T_1$	880 °C
Specific heat c	1046 J/kg K [29]
Thermal conductivity λ	1.57 J/m s K [29]
Thermal diffusivity D	5×10^{-7} m^2/s [29]
Latent heat q	4.18×10^5 J/kg [29]
$q/c\Delta T$	0.45
Young's modulus E at 20 °C	57×10^9 Pa [16]
Poisson's ratio ν at 20 °C	0.21 [16]
Thermal-expansion coefficient α at 500 °C	7×10^{-6} K^{-1} [16]
Fracture toughness K_{Ic} at 725 °C	2.25 MPa $\sqrt{\text{m}}$ [16]
Critical energy release rate $G_c=K_{Ic}^2(1-\nu^2)/E$	84.9 N/m
l_0 [Eq. (9)]	$(2.57-3.10)\times10^{-5}$ m
Velocity v	6.7×10^{-8} m/s [29]
Crack distance $2p$	1.5–4 m [1,11,14,30]
Diffusion length D/v	7.46 m
vp/D	0.1–0.27
vl_0/D	$(3.43-4.16)\times10^{-6}$

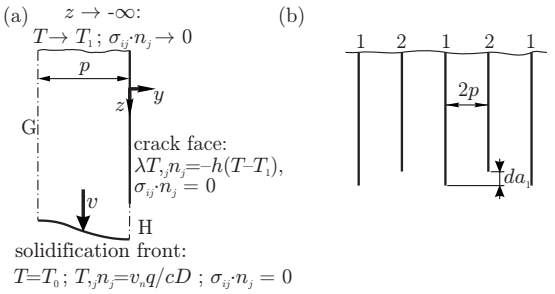

FIG. 8. (a) 2D model with solidification front and thermomechanical boundary conditions for a periodic array of straight cracks of equal length with cooling at the crack face and symmetry conditions at faces *G* and H as in Fig. 2. The solidification contour has been calculated iteratively. (b) Scheme of alternating bifurcation mode in 2D approach.

$$T(z) = T_1 + \Delta T[1 - \exp(-vz/D)]. \tag{12}$$

This temperature field has been used for the 2D bifurcation analyses in Fig. 7. For $vl_0/D \ll 1$, the result does not much differ from that obtained for the case of convective cooling through the cracks. Obviously the two calculated curves differ much from the experimental Hawaii data, $0.1 < vp/D < 0.27$ in Fig. 7, and from the values $0.2 < vp/D < 0.4$ recently derived in [18] from measured stria heights on various basalt columns.

This discrepancy has been removed by taking into account the latent heat released at the solidification front, which is free of tractions ($\sigma_{ij} \cdot n_j = 0$). This has been done with two improved temperature field models. One is based on convective cooling in porous basalt [Eq. (10)]; the other one is an extension of the model in [31] for $q > 0$, where the heat is supposed to be transferred at the crack faces (Fig. 8). In the model of Fig. 8 the contour of the solidification front with the outward normal vector n_j has been determined iteratively under the boundary condition

$$T_{,j} n_j = \frac{q v_n}{cD}, \tag{13}$$

where v_n is the normal component of the velocity vector; compare Eq. (11).

From the result that 2D bifurcation analyses differ from 3D ones only by a factor of 2 or less, as seen in Fig. 7, it can be concluded that 2D calculations are sufficient here for the interpretation of experimental data. For both models the mechanical boundary and symmetry conditions as in Fig. 8 are used. This will be discussed in detail in [36] along with problems due to the limits of the linear-elastic approach and to viscoelastic effects [16,37].

The displacement fields near the crack tip and the energy release rates have been calculated with Eqs. (7) and (6) by means of FEM for the two models. The lower theoretical curves 2D (10) and 2D for $q > 0$ in Fig. 7 follow from $G = G_c$ and 2D bifurcation criterion (A2) in Appendix A. The similarity of the two results is due to the nearly same temperature gradients near the solidification front and crack tips, corresponding to Eqs. (11) and (13), which determine the stress field near the crack tips and the energy release rate *G*.

The agreement between the Hawaii data and the critical vp/D calculated by taking into account the latent heat (Fig. 7, lower left portion) is fairly good for 2D case, considering that several uncertainties are involved. The Hawaii data [29] are regarded as uncertain within a factor of 2 [11], and the uncertainty of l_0 due to the variation in the material data with temperature may be even larger. The agreement would be even better with 3D results which would be slightly lower, as expected by comparison with the results obtained from calculations neglecting the latent heat (Fig. 7, upper portion).

VI. CONCLUSIONS

It is concluded that the relation between the diameter of basalt columns and the velocity of crack propagation can be derived from a linear-elastic fracture mechanics bifurcation analysis with simplified steady-state temperature models involving convective heat transfer either along the cracks or through porous basalt. Both temperature models give nearly the same results. By neglecting the heat released during solidification, we obtain a proportionality of column diameter and D/v, where v is the propagation velocity of the crack network forming the columns. As a remarkable detail, the diameters derived with our computable 3D model by considering a bifurcation mode compatible with observations differ from those derived with a 2D model by a mere factor of 1/2.

It has been demonstrated within the frame of this model that a smallest possible column diameter for a given propagation velocity can be derived from a bifurcation analysis for stationary crack propagation. This differs from the assumption in [27] that the diameters are essentially set at an early stage.

Fairly good agreement between theory and Hawaiian data is reached only if the heat released at the traction free solidification front is taken into account. In view of the fact that the temperature-dependent material parameters are rather uncertain and there is some scatter in the measured data, the agreement between theory and experiment can be considered satisfactory.

ACKNOWLEDGMENTS

This paper has benefited from the work of G. Müller, whose experiments with drying starch slurry furthered the understanding of basalt column formation. Thanks are due to P.-Y. Robin, whose interest in the subject encouraged us to confront the problems of a 3D bifurcation analysis. The support for this work by the Deutsche Forschungsgemeinschaft (DFG) under Contract No. BA 1411/10 is greatly acknowledged.

APPENDIX A: 2D BIFURCATION CRITERION

We consider an idealized array of propagating cracks of equal length. Depending on stability limits in Fig. 6, this or another solution is realized. As shown in [23], short-range interaction between the cracks in an array favors one particular bifurcation mode with every other crack being longer by the increment da_1, while the remaining cracks stop [alternating mode with $da_2 = 0$; see Fig. 8(b)].

In order to determine the bifurcation point as in the 3D case the increment da_2 has been kept zero. With Eqs. (4) and (5) the change in the energy release rates G_1 and G_2 for equal crack lengths $a_1=a_2$ can be written in the case of $da_1 \geq 0$ and $da_2=0$ for $dt \geq 0$ as

$$dG_1(a_1,a_2,t) = \frac{\partial G_1}{\partial a_1} da_1 + \frac{\partial G_1}{\partial t} dt = 0,$$
$$dG_2(a_1,a_2,t) = \frac{\partial G_2}{\partial a_1} da_1 + \frac{\partial G_2}{\partial t} dt \leq 0. \quad \text{(A1)}$$

Here the first equation determines da_1. With the second equation it can be checked whether $dG_2 \leq 0$ [Eq. (5)] is fulfilled or not. At the bifurcation point the equality sign is valid. Since the derivatives with respect to time t are equal for $a_1=a_2$, subtracting the equations in Eq. (A1) gives the bifurcation criterion [21,23]

$$\left(\frac{\partial G_1}{\partial a_1} - \frac{\partial G_2}{\partial a_1} \right) \Bigg|_{a_1=a_2} = 0. \quad \text{(A2)}$$

It gives those parameter combinations where the basic solution is not stable and turns into the alternating mode solution which is the stable one.

Criterion (A2) is equivalent to the numerical 3D calculation of the bifurcation point in this work. It must be mentioned that the bifurcation criterion applied in [31] does not take into account the irreversible character of crack propagation. Nevertheless it has served as a fairly good approximation.

APPENDIX B: PROCEDURE OF 3D BIFURCATION ANALYSIS

The periodicity of the problem implies the following relations between the displacements on ligament faces E and F in Fig. 4(d):

$$u_z^E = u_z^F, \quad u_s^E = -u_s^F, \quad u_n^E = -u_n^F. \quad \text{(B1)}$$

The subscripts s and n denote the directions along the s coordinate and normal to the ligament faces, respectively.

While for the highly symmetric basic solution (see Fig. 2) the stress intensity factors K_{II} and K_{III} are zero everywhere on the crack contour, they are incrementally nonzero on the less symmetric contour of the bifurcation solution in Figs. 4 and 5.

For an extension of Eq. (6) we have, according to [33],

$$G = \frac{1-\nu^2}{E}(K_{\mathrm{I}}^2 + K_{\mathrm{II}}^2) + \frac{1+\nu}{E} K_{\mathrm{III}}^2. \quad \text{(B2)}$$

The incremental change in G due to a transition from the basic contour to the bifurcation solution is

$$dG = \frac{2(1-\nu^2)}{E} K_{\mathrm{I}} dK_{\mathrm{I}} \quad \text{(B3)}$$

since the terms $K_{\mathrm{II}}dK_{\mathrm{II}}$ and $K_{\mathrm{III}}dK_{\mathrm{III}}$ vanish at the bifurcation point where $K_{\mathrm{II}}=0$ and $K_{\mathrm{III}}=0$.

As a generalization of Eq. (A1), the crack front is thought to be subdivided into small sections numbered by i which may be related to the FEM grid points. The incremental change in the energy release rate at one site i depends on the increments da_j on every other site j on the crack front, as well as on dt. This can be written with Eq. (4), as done with Eq. (A1), as

$$dG_i(a_j,t) = \frac{\partial G_i}{\partial a_j} da_j + \frac{\partial G_i}{\partial t} dt = 0. \quad \text{(B4)}$$

We make use of the fact that the partial derivative with respect to time does not depend on the incremental change in the contour. So we can take this derivative from the steady-state (ss) solution

$$dG_i^{\mathrm{ss}}(a_j,t) = \frac{\partial G_i}{\partial a_j}\Bigg|_{\mathrm{ss}} da_j^{\mathrm{ss}} + \frac{\partial G_i}{\partial t} dt = 0, \quad \text{(B5)}$$

where $da_j^{\mathrm{ss}} = v\,dt$ for all j, which makes

$$dG_i(a_j,t) = \frac{\partial G_i}{\partial a_j} da_j - \frac{\partial G_i}{\partial a_j}\Bigg|_{\mathrm{ss}} v\,dt = 0. \quad \text{(B6)}$$

In this way, unsteady temperature field calculations are avoided.

Technically, the crack contour of the basic solution is put ahead by a small distance $v\,dt$, with the temperature field kept unchanged. This makes a small contribution to G and hence a small violation of Eq. (B6), which has to be removed by iterative variation in da_j. This is done with the gradient method, and the result is $da(s)$ in Fig. 5. It has been checked that the increment chosen here, $v\,dt \approx 0.04p$, is sufficiently small so that the results in Figs. 5–7 are not affected by its size.

APPENDIX C: SCALING ARGUMENTS WITHOUT LATENT HEAT

The critical values of vp/D in Fig. 6(a) are apparently independent of the effective cooling parameter hp/λ. This numerical result is compatible with scaling arguments also applied in [38]. The line of reasoning is explained below.

For the 2D problem we define $\partial G_1/\partial a$ as the partial derivative for equal advance of both subsets of cracks at a fixed time and replace $\partial G_1/\partial a_1$ by means of bifurcation condition (A2). Since $a_1=a_2$ at the bifurcation point, we obtain

$$\frac{\partial G_1}{\partial a} \equiv \frac{\partial G_1}{\partial a_1} + \frac{\partial G_1}{\partial a_2} = \frac{\partial G_2}{\partial a_1} + \frac{\partial G_1}{\partial a_2} = 2\frac{\partial G_2}{\partial a_1} \quad \text{(C1)}$$

as an equivalent form of the bifurcation condition. Now we consider an estimate for the right-hand side due to mutual interaction of neighboring cracks: if they differ in length as seen in Fig. 8(b), the shorter ones are partly unloaded by the longer ones. As a reasonable estimate the shorter ones are essentially unloaded if the length difference is equal to their mutual distance or spacing $2p$. This means

$$\frac{\partial G_2}{\partial a_1} \approx -\frac{G_2}{p}. \quad \text{(C2)}$$

Now we consider the left-hand side in Eq. (C1). Far ahead of the crack tips the temperature is homogeneous and high, and

far behind it is homogeneous and low. The inhomogeneous temperature field near the crack tips gives rise to thermal stresses and a corresponding energy release rate.

In the case of ideal heat transfer at the crack faces, the transition length of the temperature field is given by the thermal diffusion length D/v. The same transition length applies to the thermal stress field which would be there if the temperature field were there but not the cracks. The stress field determines the energy release rate. This implies

$$\frac{\partial G_1}{\partial a} \approx -\frac{v}{D} G_1. \tag{C3}$$

In the case of poor (effective) heat transfer, which implies a jump of temperature at the interface, the transition length of the temperature field is governed by the ratio of thermal conductivity and heat transfer coefficient. If this transition length is much larger than the crack spacing, most of the temperature difference is realized far behind the crack tips where it does not give rise to thermal stresses in the separate strips. So it appears that in this case, only a small fraction of the total temperature difference contributes to thermal stresses. Hence, thermal stresses and energy release rate G_1 in Eq. (C3) are correspondingly smaller with poor heat transfer but the extension of the thermal stress field is about the same, namely, D/v, which implies, with Eqs. (C3) and (C1) and $G_1=G_2$, that the numerical result

$$vp/D = \text{const} \tag{C4}$$

in Fig. 6(a) is reproduced.

The power of 2/3 in Fig. 6(b) is derived from scaling arguments in [31]. Likewise, the result in Fig. 7, $p \sim l_0$ for $vl_0/D \gg 1$ in the presence of the temperature field [Eq. (12)], is derived in [19]. As can be seen in lower left portion of Fig. 7, the scaling behavior of the results obtained by taking into account the latent heat differs from Eq. (C4), which will be discussed in [36].

APPENDIX D: CURVED CRACK FACES AFTER BIFURCATION

Obviously, any rearrangement of the columns after bifurcation implies crack propagation with curved paths until another stationary regime is reached, as indicated by the arrows in Fig. 4(b). Such phenomenon has been tacitly assumed as a precondition of the approach taken in this paper. It can be shown that the required curvature follows from both plausible arguments and calculation of dK_{II}.

According to the peculiarity of $da(s)$ as seen in Fig. 5 (inset), the triple crack face at points 1 becomes a crack face with a kink. Generally, kinks in a crack face tend to become smoothed. (There is also experimental evidence for this, as seen in the tomogram of Fig. 4(a) and in the movies in [13], for example.)

The quantitative approach to the transient stage of curved crack propagation is based on the bifurcation mode increment $da(s)$ in Fig. 5(b) with its mode II stress intensity factor $dK_{\mathrm{II}}(s)$ as indicated in Fig. 9(a). It can be calculated, similarly as in Eq. (7), from the in-plane displacement component $du_{\mathrm{II}}(s) \sim da(s)$ normal to the crack contour in ligament direction [33] with respect to the crack tip at $r=0$:

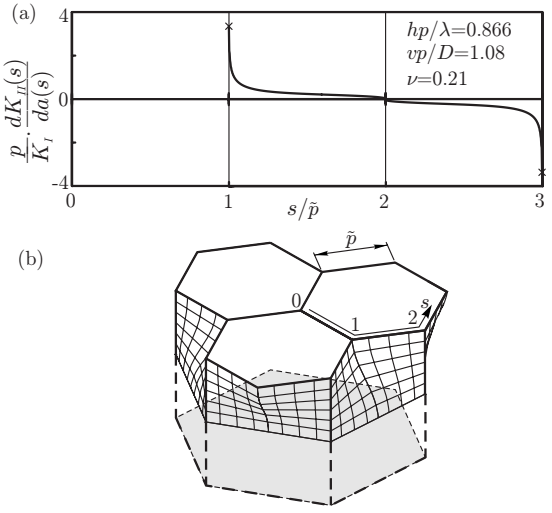

FIG. 9. (a) Incremental mode II stress intensity factor $dK_{\mathrm{II}}(s)$ related to the crack contour increment $da(s)$ at the instant of bifurcation (Fig. 5). (b) Schematic representation of three columns merging into one, with the initial curvature of the faces from Eq. (D2) due to the presence of $dK_{\mathrm{II}}(s)$ in (a).

$$dK_{\mathrm{II}}(s) = \frac{E}{4(1-\nu^2)} \lim_{r\to 0} \sqrt{\frac{2\pi}{r}} [du_{\mathrm{II}}(s,r) - du_{\mathrm{II}}(s,0)]. \tag{D1}$$

In Fig. 9(a), $dK_{\mathrm{II}}(s)$ vanishes for $0 \le s/\tilde{p} \le 1$ for reasons of symmetry; see the face labeled D in Fig. 4(d). Figure 9(b) implies a change of sign of $dK_{\mathrm{II}}(s)$ at point 2 in Fig. 4(d).

$dK_{\mathrm{II}}(s) > 0$ in the region $1 \le s/\tilde{p} \le 2$ implies an infinitesimal deflection of the crack face, which is equivalent to the onset of a finite curvature, as indicated in Fig. 9(b) and quantified by the radius of curvature, $R_n(s)$,

$$\frac{1}{R_n(s)} = -\frac{2}{K_{\mathrm{I}}} \frac{dK_{\mathrm{II}}(s)}{da_n(s)} \approx -\frac{2}{K_{\mathrm{I}}} \frac{dK_{\mathrm{II}}(s)}{da(s)}. \tag{D2}$$

Here, the circle of curvature with radius $R_n(s)$ lies in the plane normal to the crack contour of the basic solution. The above equation represents an approximate 3D extension of Eq. (104) of [39] which was the basis for simulation of 2D curved crack paths in [40]. Here $da_n(s)$ means an increment which is in the crack plane (Fig. 2) and normal to the crack contour. Because of the small slope of the basic solution [see Fig. 3(b)] $da_n(s)$ is nearly equal to $da(s)$ in Fig. 5(b), which is in z direction.

Equation (D2) provides an approach to the understanding of the observed phenomenon of three columns merging into a larger one as illustrated in Figs. 9(b) and 4(b). Also it has been shown herewith that our assumption of the bifurcation mode being confined to the direction of the basic solution does not pose a restriction.

[1] P. Budkewitsch and P.-Y. Robin, J. Volcanol. Geotherm. Res. **59**, 219 (1994).
[2] E. A. Jagla and A. G. Rojo, Phys. Rev. E **65**, 026203 (2002).
[3] J. W. French, Nature (London) **109**, 274 (1922).
[4] J. Adamovič, in *Abstracts of the Lasi II: Physical Geology of Subvolcanic Systems: Laccoliths, Sills, and Dykes*, Portree, Isle of Skye, Scotland, 1–3 April 2006, edited by K. Thomson (Springer, Berlin, 2006) [Visual Geosci. **11**, 72 (2006)].
[5] G. M. Young, J. Geol. **116**, 527 (2008).
[6] G. Müller, J. Geophys. Res. **103**, 15239 (1998).
[7] G. Müller, J. Volcanol. Geotherm. Res. **86**, 93 (1998).
[8] G. Müller, J. Struct. Geol. **23**, 45 (2001).
[9] A. Toramaru and T. Matsumoto, J. Geophys. Res. **109**, B02205 (2004).
[10] L. Goehring and S. W. Morris, Europhys. Lett. **69**, 739 (2005).
[11] L. Goehring, S. W. Morris, and Z. Lin, Phys. Rev. E **74**, 036115 (2006).
[12] T. Mizuguchi, A. Nishimoto, S. Kitsunezaki, Y. Yamazaki, and I. Aoki, Phys. Rev. E **71**, 056122 (2005).
[13] See L. Goehring, S. W. Morris, and Z. Lin, Phys. Rev. E **74**, 036115 (2006), EPAPS deposit, for movies showing the evolution of two colonnades.
[14] D. L. Peck and T. Minakami, Geol. Soc. Am. Bull. **79**, 1151 (1968).
[15] G. P. L. Walker, in *Magmatic Processes and Plate Tectonics*, edited by H. M. Prichard, N. B. W. Harris, and C. R. Neary (The Geological Society of London, London, 1993); Geol. Soc. Spec. Publ. **76**, 3 (1993); see Fig. 5 of [6].
[16] J. M. Degraff and A. Aydin, J. Geophys. Res. **98**, 6411 (1993).
[17] S. A. Kattenhorn and C. J. Schaefer, J. Volcanol. Geotherm. Res. **170**, 181 (2008).
[18] L. Goehring and S. W. Morris, J. Geophys. Res. **113**, B10203 (2008).
[19] E. A. Jagla, Phys. Rev. E **69**, 056212 (2004).
[20] A. Nishimoto, T. Mizuguchi, and S. Kitsunezaki, Phys. Rev. E **76**, 016102 (2007).
[21] S. Nemat-Nasser, S. Sumi, and L. M. Keer, Int. J. Solids Struct. **16**, 1017 (1980).
[22] H.-A. Bahr, G. Fischer, and H.-J. Weiss, J. Mater. Sci. **21**, 2716 (1986).
[23] H.-A. Bahr, U. Bahr, and A. Petzold, Europhys. Lett. **19**, 485 (1992).
[24] Z. P. Bazant, H. Ohtsubo, and K. Aoh, Int. J. Fract. **15**, 443 (1979).
[25] S. Nemat-Nasser, L. M. Keer, and K. S. Parihar, Int. J. Solids Struct. **14**, 409 (1978).
[26] D. R. Jenkins, Phys. Rev. E **71**, 056117 (2005).
[27] E. A. Jagla, Phys. Rev. E **65**, 046147 (2002).
[28] R. Saliba and E. A. Jagla, J. Geophys. Res. **108**, 2476 (2003).
[29] H. C. Hardee, J. Volcanol. Geotherm. Res. **7**, 211 (1980).
[30] M. P. Ryan and C. G. Sammis, J. Geophys. Res. **86**, 9519 (1981).
[31] T. Boeck, H.-A. Bahr, S. Lampenscherf, and U. Bahr, Phys. Rev. E **59**, 1408 (1999).
[32] *Ansys 11 User Manual* (Swanson Analysis Systems, Canonsburg, 2007).
[33] M. F. Kanninen and C. H. Popelar, *Advanced Fracture Mechanics* (Oxford University Press, New York/Clarendon, Oxford, 1985).
[34] M. Hofmann, H.-A. Bahr, T. Linse, U. Bahr, H. Balke, and H.-J. Weiss, Int. J. Fract. **141**, 345 (2006).
[35] Computer tomography images by G. Fischer, 2005 (unpublished).
[36] M. Hofmann, H.-A. Bahr, H.-J. Weiss, G. Fischer, U. Bahr, and H. Balke (unpublished).
[37] J. Lore, H. Gao, and A. Aydin, J. Geophys. Res. **105**, 23695 (2000).
[38] H.-A. Bahr, H.-J. Weiss, U. Bahr, M. Hofmann, H. Balke, G. Fischer, and S. Lampenscherf (unpublished).
[39] M. Amestoy and J. B. Leblond, Int. J. Solids Struct. **29**, 465 (1992).
[40] V. B. Pham, H.-A. Bahr, U. Bahr, T. Fett, and H. Balke, Int. J. Fract. **141**, 513 (2006).